

Three-Dimensional Perovskite Nanophotonic Wire Array-Based Light-Emitting Diodes with Significantly Improved Efficiency and Stability

Qianpeng Zhang, Daquan Zhang, Leilei Gu, Kwong-Hoi Tsui, Swapnadeep Poddar, Yu Fu, Lei Shu, and Zhiyong Fan*



Cite This: <https://dx.doi.org/10.1021/acsnano.9b06663>



Read Online

ACCESS |



Metrics & More



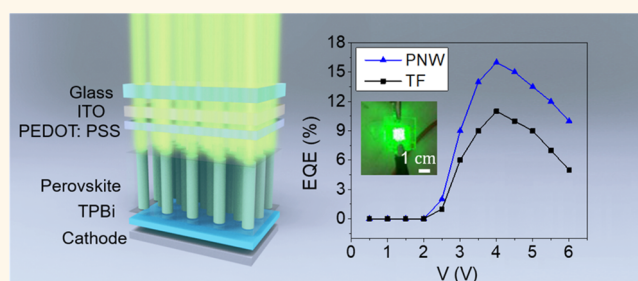
Article Recommendations



Supporting Information

ABSTRACT: Hybrid perovskites have emerged as promising candidates for highly efficient light-emitting diodes in the past few years due to their excellent crystallinity, high color purity, wide-range bandgap tunability, and solution processability. However, the reported device external quantum efficiency has not reached the level on par with that of conventional inorganic and organic light-emitting diodes. Moreover, device stability still needs substantial improvement. In this work, we demonstrate the fabrication of perovskite nanophotonic wire array-based light-emitting diodes with a capillary-effect-assisted template method. Compared with the planar control device, the nanostructured device demonstrates 45% improvement of external quantum efficiency from 11% to 16% owing to substantial enhancement on device light extraction efficiency verified by optical modeling. Intriguingly, it is also discovered that the nanostructured device possesses 3.89 times lifetime compared to the planar control device, due to effective template passivation. The results here have clearly shown that with a proper photonic device structure design, both the device performance and lifetime can be significantly improved.

KEYWORDS: perovskite, LED, nanophotonic wires, stability, bendability



Due to their high luminescent efficiency, facile solution fabrication processes, and wide tunability in emission wavelengths,^{1,2} hybrid perovskite materials have been proven as highly promising candidates for light-emitting diodes (LEDs). The external quantum efficiency (EQE) of perovskite LEDs has been improved from less than 1% to more than 20% in only four years since the first report by methods such as perovskite film morphology control and material passivation.^{3–5} Recently, researchers discovered that most current device structure designs have low light extraction efficiency which has become a major limiting factor for overall device performance.^{4,6–9} To address this issue, Y. Cao et al. utilized self-formed submicrometer disk-like structures which could passivate the surface defects and improve the light extraction at the same time,⁴ and they demonstrated 20% EQE device with 70% photoluminescence quantum yield (PLQY) and 30% light extraction.

Moreover, in our previous report, a systematically designed nanophotonic substrate comprised of the nanodome light coupler and nanowire optical antennas can significantly improve the light extraction capability, and the EQE of methylammonium lead bromide (MAPbBr₃) LED devices was increased twice with our nanophotonic substrate compared to

the planar control.⁶ Intriguingly, according to our simulations, the nanodomains alone can improve the light extraction efficiency to about 30%,⁶ and this is consistent with a recent report which utilized moth-eye structures and achieved 28% EQE for green light perovskite LED.¹⁰ As a comparison, EQE higher than 50% has already been achieved for green light organic LEDs (OLEDs).¹¹ Therefore, there is still substantial room to improve the EQE of perovskite LEDs with further study on light extraction optimization. Besides the light extraction issues in perovskite LEDs, another bottleneck problem is the long-term operational stability. Although the T_{50} has been mentioned in some recent reports,^{4,5,12–15} the testing standards are not consistent among various reports. Especially, for the cesium lead bromide (CsPbBr₃) based green light LED, devices showed lifetimes around 10 min when the maximum luminance was around 7000 cd m⁻².⁵ A longer

Received: August 22, 2019

Accepted: January 16, 2020

Published: January 16, 2020

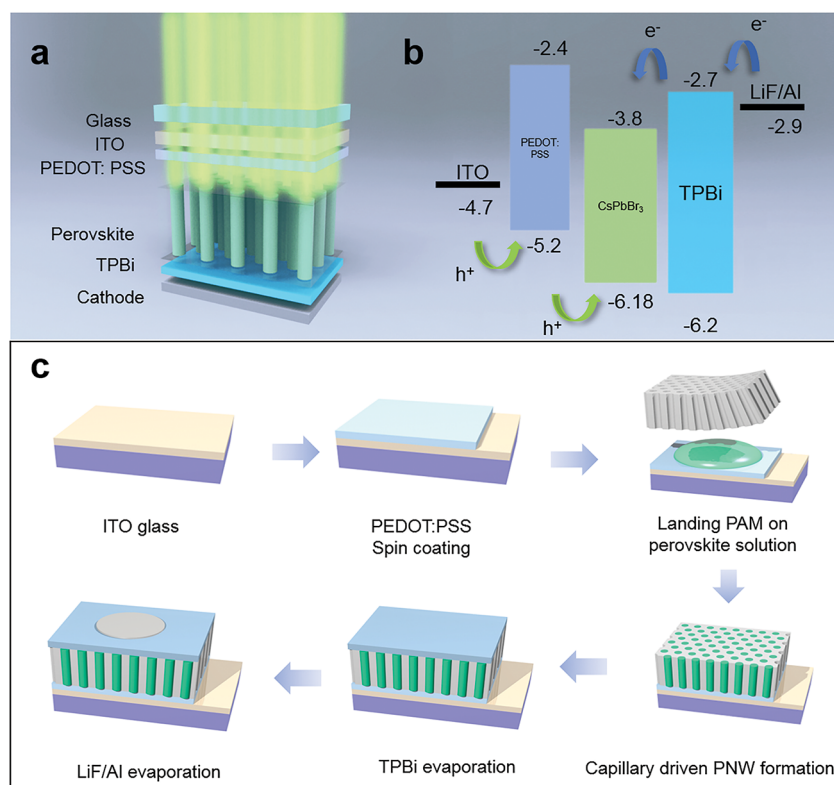


Figure 1. Perovskite nanophotonic wire (PNW) LED device structure and fabrication process. (a) Diagram of the PNW LED device. (b) Band energy diagram of the PNW LED device. (c) Fabrication process of the PNW LED device.

lifetime could be achieved if the low testing luminance around 100 cd m^{-2} was used, but it is believed that the lifetime at high luminance conditions is more meaningful. Moreover, the reported tests were usually done in a glovebox filled with nitrogen. Therefore, there is still a long way to go before perovskite LEDs can be widely accepted in display or lighting industries.

Note that most reports regarding the perovskite LED stability focused on material and interface engineering. In this work, we demonstrate a capillary-effect-assisted solution (CEAS) method for the fast growth of perovskite nanophotonic wire (PNW) arrays in a porous alumina membrane (PAM). With this method, the geometry of the nanophotonic wires can be engineered by controlling the PAM fabrication conditions. After that, PNWs were made into LEDs. Intriguingly, the LED devices showed both much higher EQE and better operational stability than the planar control device. Particularly, EQE for a PNW device was substantially increased to 1.45 times compared to thin film (TF) control, from 11% to 16%. Finite-difference time-domain (FDTD) modeling confirmed that the light extraction efficiency of the PNW device is significantly higher than that of the planar control device owing to the leaky mode behaviors in the PNWs at the emission wavelength. Moreover, the PNW device was found out to be more than 2.85 and 3.89 times stable than the TF control for the continuous lighting test with and without additional packaging at high luminance condition (peak luminance about $10\,000 \text{ cd m}^{-2}$), respectively. The significant stability enhancement can be attributed to the template protection of PNWs against water and oxygen lateral invasion which is one of the bottleneck problems undermining perovskite material stability. In addition, as the CEAS method is generic and has the minimal requirement on the holding

substrate, we have fabricated flexible PNW LEDs on indium-doped tin oxide/polyethylene terephthalate (ITO/PET) substrates. Interestingly, the PNW device also showed much better mechanical robustness than the TF control with much better endurance to the small bending radius and multiple bending cycle tests. This is also due to effective protection for the PNWs provided by a robust and flexible template of PAM. It is worth pointing out that the PNW fabrication method reported here can be extended to the fabrication of the nanowires made from many other perovskite materials. The nanophotonic design can be also adopted for other perovskite material based optoelectronic devices such as solar cells and photodetectors to achieve significant enhancement on both device performance and stability.

RESULTS AND DISCUSSION

Figure 1 shows the PNW device structure and the fabrication process. The device structure from top to bottom includes indium-doped tin oxide (ITO) glass, poly(3,4-ethylene dioxythiophene)-poly(styrenesulfonate) (PEDOT:PSS), MABr modified CsPbBr_3 PNW, 2,2',2''-(1,3,5-benzinetriyl)-tris(1-phenyl-1H-benzimidazole) (TPBi), and LiF/Ag, as shown in Figure 1a. Figure 1b shows the energy band diagram of the device where PEDOT:PSS and TPBi work as the hole injection layer (HIL) and the electron injection layer (EIL), respectively. In this work, a CEAS method is used to fabricate PNW arrays, and the fabrication process is shown in Figure 1c. The details can be found in the Methods section. Note that the key step is to use a PAM to cover perovskite solution on the substrate to allow the perovskite solution to go into the nanopores via capillary effect, thus forming a PNW array embedded in the PAM. Figure 2a is the cross-sectional

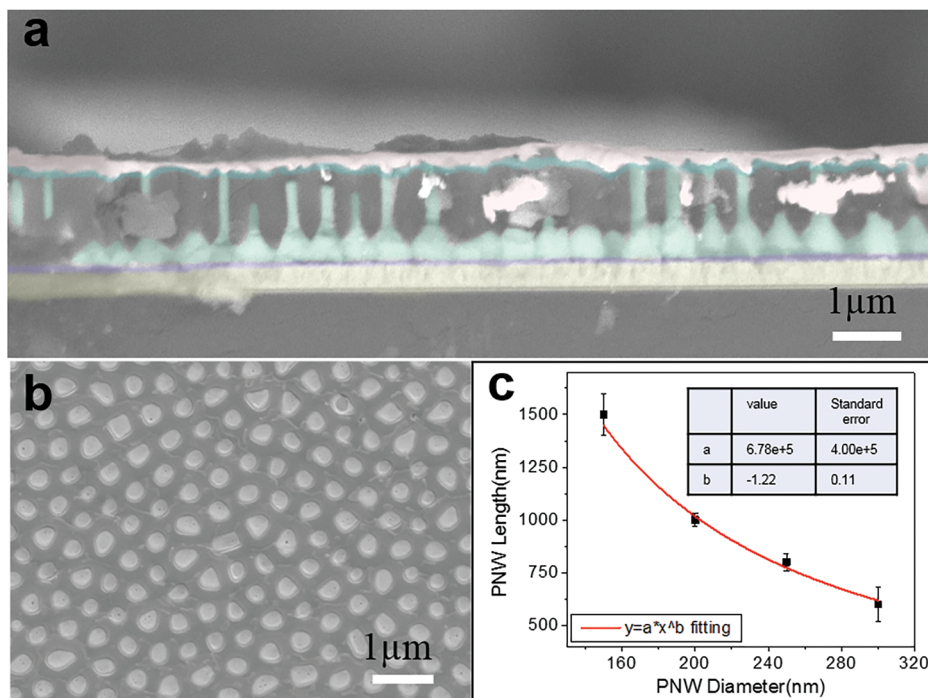


Figure 2. Device SEMs and PNW length dependence on diameters with capillary-effect-assisted solution (CEAS) method. (a) Cross-sectional SEM image of the PNW device. (b) Top view of the PNWs filled in PAM. (c) Relation curve between PNW length and diameter with the CEAS method. The scale bars in a and b are 1 μm .

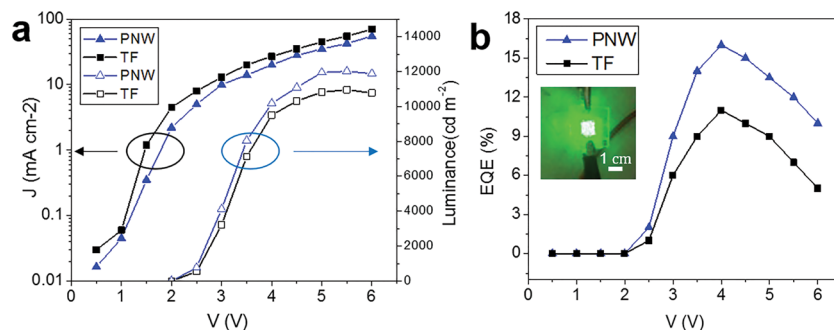


Figure 3. Device performance. (a) Current density–voltage (J – V) and luminance–voltage (L – V) curves of PNW and TF devices. (b) EQE curves of the PNW and TF devices. Inset figure: a PNW LED device at 4 V voltage, with a device area of 1 cm^2 .

scanning electron microscopy (SEM) image of a complete PNW device. The PNWs here have a length of 890 nm and a diameter of 220 nm. There is a funnel shape layer with a height of 530 nm at the lower part of the PNWs, which is the result of the funnel shape pore entrance of the PAM. This funnel shape layer can help to improve the contact with the bottom PEDOT:PSS layer for efficient hole injection. Also, the top surface of the PAM has been treated with ion milling in order to achieve a smooth surface. With a smooth top surface, good contact between PNWs and TPBi can be formed for electron injection if the PNW can reach the PAM top. Figure 2b is a top view SEM image that shows a good filling ratio of PNWs in the PAM pores. Intriguingly, it is found that, with the CEAS method, there is a maximum PNW length in the PAM which is controlled by the PAM pore size. As the PAM pore size is simply equal to the PNW diameter, the relation between the PNW length and the diameter is plotted in Figure 2c. In order to achieve this relation, we used the PAM with sufficient thickness to accommodate PNWs with different maximum lengths. Figure S1 shows the SEMs of the PNWs when

different PAM pore sizes were used. The details for pore size control can be found in the Methods section. The PNW lengths can be fitted well with Jurin's law, which is commonly used to describe the capillary effect. Simply speaking, the PNW length y follows an exponential decay $y = ax^b$ when the PAM pore size x increases. Here the fitting parameters are $a = 6.78 \times 10^5$ and $b = -1.22$. This result clearly uncovers that the PNW formation inside the PAM nanopores is driven by a capillary force while a step of spin coating is required to remove the extra amount of perovskite between the PAM and the substrate. (Figure S2 shows the transmission electron microscopy (TEM) image of a PNW with 200 nm diameter and the absorption and photoluminescence (PL) spectra. Figure S3 shows the X-ray diffraction (XRD) of the PNW.) This method to form perovskite nanowires is facile, scalable, and generic. It can be adopted to any solution processable perovskite material system for a variety of device applications such as LED, solar cells, photodetectors, etc.

In our work, the PNW arrays were assembled into LED devices and characterized, and TF LED devices were also

Table 1. Recent Reports on Perovskite LED Performance Enhancement with Different Light Extraction Strategies

work	light extraction strategy	performance enhancement
Y. Cao et al. ⁴	self-formed nanodisks	EQE more than 20% (green); light extraction efficiency from 20% to more than 30% (1.5 times enhancement)
Y. Shen et al. ³⁶	moth-eye ZnO injection layer + half-ball lens	EQE 28.2% (green)
L. Zhao et al. ⁹	thin emissive layer	EQE 17.6% (IR)
S. Jeon et al. ⁸	nanohole array with high-index contrast	peak EQE 14.6% (red/near IR); 1.64 times light extraction enhancement
Q. Zhang et al. ⁶	nanophotonic substrate (light coupler + optical antennas)	EQE from 8.19% to 17.5% (green) (twice EQE enhancement), 2.1 times enhancement; light extraction efficiency from 10–20% to more than 70% (3.5–7 times enhancement)
this work	perovskite PNWs	EQE from 11% to 16% (green) (1.45 times enhancement); light extraction from 10–20% to 40–50% (2–5 times)

Table 2. Light Extraction Coefficient (EC) of PNWs with Different Geometries, Dipole Positions, and Dipole Polarization Directions^a

PNW geometry	dipole polarization	EC					average EC
		D50	D500	D1000	D1500	D1950	
P1000D400	HD	69%	65.6%	61.2%	71%	68%	44%
	VD	15.7%	12.7%	28.5%	19.3%	24.3%	
P500D200	HD	50%	54%	62.7%	63%	34%	51%
	VD	41.4%	60.6%	48.2%	30%	66.4%	

^aThe average results are from the 10 different dipole cases for each geometry. P1000D400 means 1000 nm pitch and 400 nm diameter. P500D200 means 500 nm pitch and 200 nm diameter. HD means horizontal dipole, and VD means vertical dipole. D50, D500, D1000, D1500, and D1950 mean the dipole depths of 50 nm, 500 nm, 1000 nm, 1500 nm, and 1950 nm, respectively.

fabricated as control samples. Figure 3 shows the device performance characterization for both the PNW LED and the TF LED. The luminance (L) and current-density (J) vs voltage (V) curves are shown in Figure 3a. The devices were driven in voltage mode. It can be seen that turn-on voltages for both PNW and TF LEDs are around 2.5 V. Intriguingly, with the same driving voltage, PNW devices always have lower current density than TF devices. This can be simply attributed to the fact that the PNW array has a larger internal resistance than TF due to less perovskite material filling in the device. For the TF device, the current density at 4 V is 27 mA cm⁻², but for the PNW device the current density is only 20 mA cm⁻². Moreover, the PNW device can give a luminance of 12 016 cd/m² at 5.5 V. However, the TF device only gives 10 953 cd/m² at the same voltage. Thus, the maximum luminance was enhanced by 9.7%. Although the luminance enhancement for PNW is not substantial compared to the TF control, the EQE enhancement is significantly higher owing to much lower current density for the PNW device. Figure 3b shows the EQE curves for the PNW and TF devices. The inset of Figure 3b is a photograph of a PNW device working at 4 V with 1 cm² actual emission area. Eventually, the best EQEs for the PNW and TF devices are 16% and 11%, both at 4 V. Here we attribute the 45% EQE improvement for the PNW device to the significant light extraction enhancement, and the following paragraphs will provide a detailed analysis supported by optical simulations. (Table 1 gives a comparison between our work and the state-of-art reports on PeLEDs with light extraction enhancement. Moreover, the corresponding light extraction strategies and the results of enhancement are also included. The 1.45 times EQE enhancement is comparable to the state-of-art reports.)

To acquire an in-depth understanding of the large EQE enhancement for PNW LEDs, we performed optical modeling with the FDTD method. The schematic for the dipole positions and polarization directions is shown in Figure S4.

Considering the PNW length is 2000 nm, a dipole depth 50 nm (D50) means the dipole is just below the top surface of the PNW, and a depth of 1950 nm (D1950) means the dipole is just above the bottom surface of the PNW. The light extraction was calculated according to the methods discussed in our previous work.⁶ More simulation details can be found in the Methods section. Table 2 shows the calculated light extraction coefficient (EC) which is the ratio of output light power (collected by the plane monitor in the out space) over the source power (collected by the box monitor surrounding the dipole source). A better understanding of the light–matter interaction inside the PNWs can be obtained with the EC. Five dipole positions and two dipole polarization directions were considered for each geometry, and the average EC results are from the 10 cases for each geometry. To verify the convergence of this method, we used the P500D200 PNWs as an example and used 38 dipole positions on the axis. For this case, the average extraction coefficient (EC) is 52.7%, as shown in Table S1, Supporting Information. Furthermore, we simulated another 38 dipole positions of half radius distance shifted away from the axis, and the average EC now is 50.5%. Both 52.7% and 50.5% are close to the result (average 51% from 10 dipoles), as we show in Table 2. For the device with P1000D400 PNW, horizontal dipoles (HDs) always yield good EC (from 61.2% to 71%) while the vertical dipoles (VDs) lead to poor EC (from 12.7% to 28.5%). However, for the device with P500D200 PNW, the EC does not show a clear preference to the dipole polarization. Figure S5 shows the cross-sectional E^2 patterns for the P1000D400 and P500D200 PNWs with different dipole positions and polarization directions. Figure S6 shows the normalized E^2 patterns at the PNW emitter top for the P1000D400 and P500D200 PNWs with different dipole positions and polarization directions. The nanophotonic effects are complex here, and more than one type of possible resonance (surface lattice resonance, Fabry–

Perot resonance, etc.) are involved in the process,^{16–18} which needs more comprehensive study in the future.

After we consider all 10 cases for dipoles and calculate the average EC for PNWs with two different geometries, we found that the P500D200 PNWs show a better average EC than P1000D400 PNWs. It is known that the EC for a perfect flat TF structure is around 10% as reported in our previous work;⁶ the PNWs have shown the light extraction enhancement with a factor about 4 to 5 times.

Figure 4a1–a4 shows the cross-sectional E^2 intensities of PNWs with (a1) P1000, D1000, and HD, (a2) P1000, D1000,

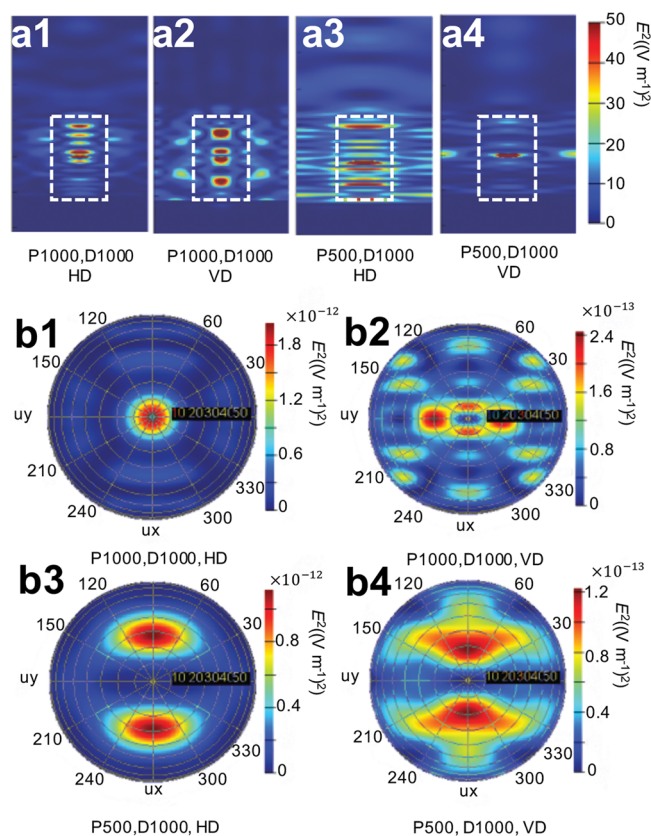


Figure 4. Cross-sectional E^2 intensity profiles for (a1) P1000, D1000, and HD, (a2) P1000, D1000, and VD, (a3) P500, D1000, and HD, and (a4) P500, D1000, and VD. Far-field E^2 intensity profiles for (b1) P1000, D1000, and HD, (b2) P1000, D1000, and VD, (b3) P500, D1000, and HD, and (b4) P500, D1000, and VD. P1000: pitch 1000 nm; D1000: dipole depth 1000 nm; HD: horizontal dipole direction; VD: vertical dipole direction; P500: pitch 500 nm.

and VD, (a3) P500, D1000, and HD, and (a4) P500, D1000, and VD. Here P500, P1000, D1000, HD, and VD represent pitch 500 nm, pitch 1000 nm, dipole depth 1000 nm, horizontal dipole direction, and vertical dipole direction, respectively. The dipole depth in the PNW is 1000 nm, which is the case when the dipole is at the center of the PNW. All the figures have the same color bar range to make a fair comparison on E^2 field patterns of both inside and outside the PNWs among different cases. According to Table 2, the EC for P1000D1000 HD is 61.2% and is 28.5% for P1000D1000 VD. Figure 4b1–b4 shows the far-field E^2 intensities for PNWs with (b1) P1000, D1000, and HD, (b2) P1000, D1000, and VD, (b3) P500, D1000, and HD, and (b4) P500, D1000, and

VD. Far-field E^2 intensities for HD are about 10 times higher than those of VD. Moreover, Figure S7 and Figure S8 show the normalized E_z and H_z components at the PNW emitter top for P1000 and P500 PNWs with different dipole depths and dipole polarization directions. As all the modes at 530 nm in Figure S7 and Figure S8 have both E_z and H_z components, we categorize all the modes as hybrid leaky modes. According to L. Cao et al., optical modes in nanoscale resonators are often very leaky, namely, they radiate efficiently.¹⁹ For leaky modes, energy can escape from the open system.

Another common mode type in high index nanowires is the Mie resonance mode.^{20–23} The index of the perovskite PNW at the emission wavelength (530 nm) is 2.2.²⁴ As for the high-index dielectric cylinders, the Mie resonance happens at wavelength $\lambda_{\text{Mie_Res}} = \frac{m \cdot \pi D}{n}$, where $\lambda_{\text{Mie_Res}}$ is the resonance wavelength inside the high-index dielectric, m is an integer, D is the diameter of the cylinder, and n is the refractive index of the cylinder.²¹ For nanowires ($n = 2.2$) with 400 and 200 nm diameters, Mie resonance can happen around 570 nm in the ideal case. Considering we have nanowire arrays embedded in alumina, the precise Mie resonance wavelength position is not straightforward to get but can fall in the 500 to 600 nm range.

Moreover, Figure S9 shows far-field E^2 intensity patterns for different dipole positions and polarization directions. The simulated far-field patterns for P1000 PNWs are more complicated than those for P500 PNWs because of the existence of the high order diffractions in the P1000 PNWs. The far-field patterns can be used to analyze the modes inside the nanowires. Taking the isolated single nanowire, for example, for lowest order guided mode HE_{11} , far-field intensity is the strongest in the center; however, for higher order guided modes, far-field intensity is minimal in the center.¹⁷ In a real case, the far-field intensity is more complicated and will be a superposition of each mode, and the leaky modes radiating from nanowire sidewalls need also be considered. Therefore, a potential application of the theoretical far-field patterns study can help people reversely analyze the emitting position and the emitting dipole polarizations in the nanowires.

Another interesting effect is the PNW length effect. We did more systematic simulations and studied PNWs with lengths of 500, 1000, and 1500 nm, respectively. The results are added as Figure S10. As shown in Figure S10a, the P1000D400 PNWs with length of 500 nm can have a theoretical average extraction efficiency of 74%. The extraction efficiency for PNWs with length of 1000 nm (33.7%) and 1500 nm (53.3%) do not show a significant difference with that for PNWs with length of 2000 nm (44%). Figure S10b is the result for P500D200 PNWs, and the average results for different lengths are very close. Like the case for P1000D400 PNWs, P500D200 PNWs also have the best extraction efficiency when the length is 500 nm. However, in practice, when the PNW length is 500 nm, the PAM film is too fragile to handle for device fabrication. Nevertheless, the theoretical study here for the length effect is still quite meaningful and can give guidance for future study with an optimized fabrication process for PNW based LED devices.

Note that although there is 4 to 5 times enhancement in light extraction from a TF device to a PNW device according to optical modeling, the luminance and EQE enhancements of a real device were only about 1.5 times as shown in Figure 3. We ascribed this discrepancy to the loss of internal quantum efficiency (IQE). One possible IQE loss mechanism is that it is more difficult to form perfect interfaces between the emitter

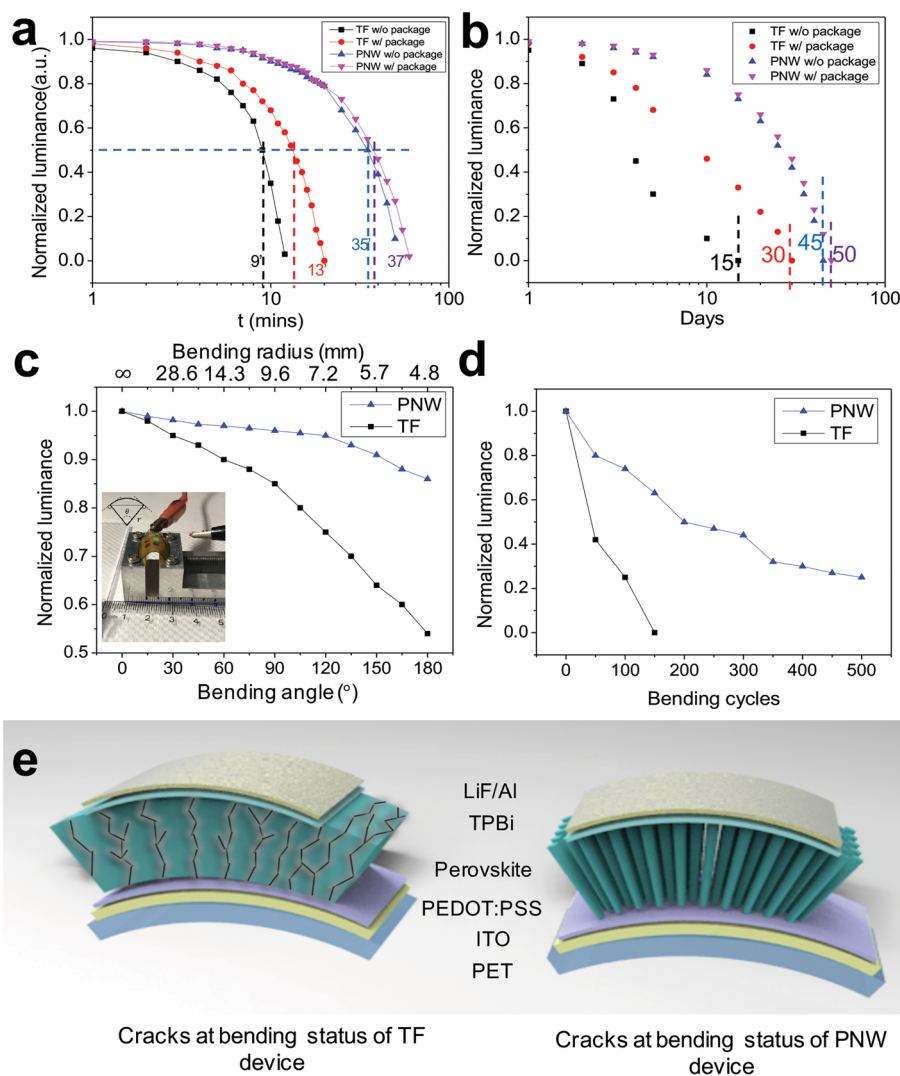


Figure 5. Stability and mechanical robustness. (a) Continuous lighting (at 4 V) stability of the PNW and TF devices with and without epoxy packaging. T_{50} for TF without packaging, TF with packaging, PNW without packaging, and PNW with packaging are 9, 13, 35, and 37 min, respectively. (b) Noncontinuous lighting (at 4 V) stability of PNW and TF devices with and without epoxy packaging. (c) Bending test of PNW and TF devices with different bending angles. Inset figure: the LED device working at bending status. The circular electrode is connected by a copper wire. (d) Mechanical robustness test of NW and TF devices after certain bending cycles. (e) Crack mechanism diagram of the TF and PNW devices.

layer and injection layers in PNW devices than in TF devices due to the limited contact area.

Previously, we have discovered that PAM templates can protect the perovskite nanowires from fast degradation mainly by preventing the lateral diffusion of water and oxygen molecules.^{25,26} In this work, stabilities of the PNW and TF LED devices were evaluated, and the results are shown in Figure 5. Figure 5a is the device stability under continuous emission mode. Both PNW and TF devices were driven by 4 V voltage. The luminance of the PNW device with and without NOA81 UV epoxy packaging dropped to 50% at 37 and 35 min, respectively (as this time is also named as T_{50} of the device). Because the testing luminance is pretty high (peak luminance more than $10\,000\text{ cd m}^{-2}$), our PNW device T_{50} is respectably long compared to those of the reported state-of-art perovskite LED devices (Table S2, Supporting Information). The T_{50} values for thin-film control with and without packaging were only 13 and 9 min, respectively. Therefore, the PNW device shows 2.85 times and 3.89 times longer

lifetimes than the TF control, respectively. This enhancement in the continuous light stability can be attributed to PAM protection of the PNWs against the water and oxygen diffusion. That is also why the PNW device shows more lifetime enhancement when packaging was not applied. Figure 5b is a long-term stability comparison. The luminance of the PNW and TF devices with and without packaging was measured in the air (with $\sim 70\%$ humidity) once a day with 4 V voltage. After the measurement, the devices were stored back into the glovebox filled with nitrogen. The PNW devices with and without packaging eventually failed to work after 50 and 45 days, respectively. As a comparison, the TF devices with and without packaging stopped working after 30 and 15 days, respectively. This means the packaging can prolong the storage time for the TF device twice, and the lateral protection from the PAM which separates the PNWs apart is more effective in terms of increasing the storage time for perovskite LEDs. That is because the PAM template shuts down the lateral pathway for water molecule diffusion, leading to the

enhanced long-term stability in PNW LEDs. It is worth noting that Joule heating is also one important cause for the short lifetime of the perovskite LED devices (the other two main causes are ion migration and moisture degradation).^{9,27} As Joule heating is generated when currents pass through the defects, the Joule heating is related at the defect level. Besides improving material quality, designing the balanced carrier injections can help to reduce the current level and thus reduce the Joule heating.²⁸ Intriguingly, Z. Wei et al. reported that Joule heating induced crystal annealing can reduce device resistance and enhance luminance output.²⁹ That means Joule heating is not always hurting the device. Moreover, because Al_2O_3 ($30 \text{ W m}^{-1} \text{ K}^{-1}$) has a much higher thermal conductivity than perovskite ($0.46 \text{ W m}^{-1} \text{ K}^{-1}$),³⁰ the PAM can help the PNW with heat dissipation in our case. As our work improves the device stability mainly by the template passivation, we believe longer lifetime (more than 30 min) can be achieved if the Joule heating problem can be alleviated in the future.

In addition to demonstrating performance and stability enhancement, flexible PNW LEDs have been successfully fabricated on ITO/PET substrates, as the PNWs are well embedded in thin PAM with excellent flexibility.³¹ The flexible LEDs can potentially find applications for flexible displays in the future. The bendability of typical flexible PNW devices has been characterized, and the results are shown in Figure 5c,d. As shown in Figure 5c, when it was bent to 180° , the PNW device remains at 86% luminance. However, the TF device only showed 54% of the original luminance. Furthermore, when the device was bent up to 500 cycles (with 180° bending angle), the PNW device still had 25% of the original luminance, while the TF device stopped working after 150 cycles, as shown in Figure 5d. This dramatic improvement on bendability for the PNW LED can be rationalized by considering the fact that each individual PNW is separately surrounded by aluminum oxide packaging material which has excellent mechanical robustness, thus bending the device does not introduce any crack line inside the PNWs as long as the PAM holds (Figure 5e). However, the polycrystalline perovskite TF has many grain boundaries which are weak points prone to generate crack lines when the device is bent to a certain degree (Figure 5e). Once crack lines are generated within the film, they may also lead to the formation of crack lines in the charge transporting layers and electrodes that sandwich the perovskite layer. (Figure S11 shows the optical photos of the bending TF and PNW devices.)

CONCLUSIONS

In this work, we report a facile and scalable method to grow high-quality PNW arrays in PAM templates. The PNW arrays were assembled into LED devices which showed more than 45% improvement on EQE over the TF control device. The enhancement in device performance can be attributed to the enhanced light extraction efficiency in PNW devices which possess leaky mode behavior at the emission wavelength. More importantly, the PAM template provides lateral protection of perovskite materials from moisture diffusions; therefore, the PNW devices showed 2.85 and 3.89 times T_{50} enhancement compared to the TF control device with and without packaging, respectively. In addition, flexible PNW LEDs were also fabricated, and it was found that PNW devices have much better mechanical robustness and bendability as compared with the TF counterparts. Overall, the combination of PNW and the surrounding oxide template addresses critical issues on

performance and stability at the same time. The device fabrication process developed here can be adopted to any solution-processable perovskite material system for achieving performance enhancement for a variety of device applications such as LED, solar cells, photodetectors, etc.

METHODS

Materials. CsBr, MABr, PbBr_2 , DMSO, PEDOT:PSS, TPBi, and LiF were purchased from Sigma-Aldrich. MABr, CsBr, and PbBr_2 were dissolved in DMSO with 0.5:1:1 molar ratios as perovskite precursors.

Through-Pore Free-Standing PAM Preparation. The free-standing PAM was prepared by a two-step anodic anodization method, and the details can be found from our previous works.^{6,32–35} Note that the PAM thickness was controlled by the second anodization time, and the PAM pore diameter was controlled by the second etch time. A 200 V anodization voltage was used to generate a pitch of 500 nm. To make the free-standing PAM through-pore, the barrier side of the PAM was removed by ion milling with a 750 V voltage and 85° tilted angle for 1 h.

PNW Device Fabrication. An ITO glass was consecutively cleaned with acetone, isopropyl alcohol, and deionized water with 5 min of sonication in each step. O_2 plasma treatment was performed for 10 min. After that, the PEDOT:PSS solution was spin coated onto the ITO glass at 3000 rpm for 50 s. Then PEDOT:PSS was annealed at 150°C for 10 min. After that, 50 μL of perovskite solution was dropped onto the PEDOT:PSS. Then the through-pore free-standing PAM was placed onto the perovskite solution. Then the sample was moved onto a spin coater and rotated at 500 rpm for 5 s and then 4000 rpm for 50 s. Then the sample was baked at 60°C for 5 min to completely evaporate the DMSO. After that, TPBi with thickness around 30 nm was thermally evaporated onto the PAM top. Then 2 nm LiF and 80 nm Al were thermally evaporated with shadow masks. For high efficiency devices, the circular mask with an opening diameter of 2 mm was used. The packaging/encapsulation was realized by covering a layer of NOA-81 UV epoxy followed by 10 min of UV curing. For the circular electrode device, silver paste and copper wires were applied to the electrodes before the packaging. For flexible PNW LED fabrication, the ITO glass was replaced by ITO/PET substrate. Special care should be taken with the PEDOT:PSS annealing process for flexible device fabrication, and the temperature increase should be as slow as 10°C per 5 min to avoid the bending of PET due to the different thermal expansion coefficients between ITO and PET.

TF Device Fabrication. The fabrication process for the TF device was the same as for the PNW device except for the perovskite deposition step. For the TF perovskite deposition, the spin coating condition was 3000 rpm for 1 min. A total of 50 μL of perovskite solution was dropped onto the PEDOT:PSS at the 10th second of the spin coating. A total of 100 μL of toluene was dropped onto the perovskite at the 50th second of the spin coating for anti-solvent (nanocrystal pinning) purpose. No postannealing was required for the TF perovskite deposition as the solvent evaporates more quickly in this case compared to the PNWs.

LED Measurement. LED devices were driven with a Keithley 2400 with a voltage source. Luminance and EQE were measured with an Ocean Optics Flame spectrometer and an integrating sphere. The spectrometer was calibrated by a standard source as reported in our previous work.⁶

Optical Modeling. Optical modeling was done with the finite-difference time-domain method (Lumerical FDTD package). Detailed procedures follow our previous report.⁶ Simulation is done with a single wavelength to avoid the inaccuracy caused by material index fitting. A periodic boundary condition is used on the x and y directions to form the PNW array. A PML condition is used on the z direction. Dipole sources with both horizontal and vertical resonance directions are used to simulate the point light source. A power transmission box surrounding the dipole source is used to record the source power. A plane monitor above the device is used to record the

output power and analyze the far-field pattern. Material indexes for Al_2O_3 (Palik, 0–2 μm) and Ag (Palik) are from the built-in database in the Lumerical FDTD software package. The Br perovskite index is from M. S. Alias's work.²⁴ As for TPBi, n is 1.7 and k is 0. As for PEDOT:PSS, n is 1.5 and k is 0.⁶ The ITO index is from the Web site refractiveindex.info. For PNW simulation, the PNW length is 2000 nm. Moreover, the diagram showing the settings can be found in Figure S4, Supporting Information.

ASSOCIATED CONTENT

Supporting Information

The Supporting Information is available free of charge at <https://pubs.acs.org/doi/10.1021/acsnano.9b06663>.

Additional SEM images, nanowire characterization (TEM, UV-vis, PL, and XRD), simulation settings, cross-sectional E^2 intensities, normalized E^2 patterns at the PNW emitter top surface, normalized E_z and H_z patterns, far-field E^2 intensities, length effect study, device photos, simulation convergence verification, and device performance comparison with other reports (PDF)

AUTHOR INFORMATION

Corresponding Author

Zhiyong Fan – The Hong Kong University of Science and Technology, Hong Kong SAR, China, and HKUST-Shenzhen Research Institute, Shenzhen, China; orcid.org/0000-0002-5397-0129; Email: eezfan@ust.hk

Other Authors

Qianpeng Zhang – The Hong Kong University of Science and Technology, Hong Kong SAR, China

Daquan Zhang – The Hong Kong University of Science and Technology, Hong Kong SAR, China, and HKUST-Shenzhen Research Institute, Shenzhen, China

Leilei Gu – The Hong Kong University of Science and Technology, Hong Kong SAR, China, and HKUST-Shenzhen Research Institute, Shenzhen, China

Kwong-Hoi Tsui – The Hong Kong University of Science and Technology, Hong Kong SAR, China

Swapnadeep Poddar – The Hong Kong University of Science and Technology, Hong Kong SAR, China

Yu Fu – The Hong Kong University of Science and Technology, Hong Kong SAR, China, and HKUST-Shenzhen Research Institute, Shenzhen, China

Lei Shu – The Hong Kong University of Science and Technology, Hong Kong SAR, China

Complete contact information is available at: <https://pubs.acs.org/doi/10.1021/acsnano.9b06663>

Author Contributions

Z.F. conceived the idea. Z.F. and Q.Z. designed the experiments. Q.Z. and D.Z. fabricated devices and performed measurements. Q.Z. and K.-H.T. conducted simulations and optical analysis. S.P., L.G., Y.F., and L.S. contributed to the material characterizations. Q.Z. and Z.F. wrote the manuscript. All authors contributed to the results discussions and agree to the results.

Notes

The authors declare no competing financial interest.

ACKNOWLEDGMENTS

Q.Z. thanks Mr. X. Qiu for technical help in PAM fabrication. This work was supported by National Natural Science Foundation of China (Project No. 51672231), Shen Zhen Science and Technology Innovation Commission (Project No. JCYJ20170818114107730), HKUST Fund of Nanhai (Grant No. FSNH-18FYTRI01), and Hong Kong Research Grant Council (General Research Fund Project No. 16237816, 16309018). The authors also acknowledge the support from the Center for 1D/2D Quantum Materials and the State Key Laboratory on Advanced Displays and Optoelectronics at HKUST.

REFERENCES

- (1) Xiao, Z.; Kerner, R. A.; Zhao, L.; Tran, N. L.; Lee, K. M.; Koh, T.-W.; Scholes, G. D.; Rand, B. P. Efficient Perovskite Light-Emitting Diodes Featuring Nanometre-Sized Crystallites. *Nat. Photonics* **2017**, *11*, 108–115.
- (2) Zhang, F.; Zhong, H.; Chen, C.; Wu, X.-g.; Hu, X.; Huang, H.; Han, J.; Zou, B.; Dong, Y. Brightly Luminescent and Color-Tunable Colloidal $\text{CH}_3\text{NH}_3\text{PbX}_3$ (X = Br, I, Cl) Quantum Dots: Potential Alternatives for Display Technology. *ACS Nano* **2015**, *9*, 4533–4542.
- (3) Tan, Z.-K.; Moghaddam, R. S.; Lai, M. L.; Docampo, P.; Higler, R.; Deschler, F.; Price, M.; Sadhanala, A.; Pazos, L. M.; Credgington, D.; et al. Bright Light-Emitting Diodes Based on Organometal Halide Perovskite. *Nat. Nanotechnol.* **2014**, *9*, 687–692.
- (4) Cao, Y.; Wang, N.; Tian, H.; Guo, J.; Wei, Y.; Chen, H.; Miao, Y.; Zou, W.; Pan, K.; He, Y.; Cao, H.; Ke, Y.; Xu, M.; Wang, Y.; Yang, M.; Du, K.; Fu, Z.; Kong, D.; Dai, D.; Jin, Y.; Li, G.; Li, H.; Peng, Q.; Wang, J.; Huang, W. Perovskite Light-Emitting Diodes Based on Spontaneously Formed Submicrometre-Scale Structures. *Nature* **2018**, *562*, 249–253.
- (5) Lin, K.; Xing, J.; Quan, L. N.; de Arquer, F. P. G.; Gong, X.; Lu, J.; Xie, L.; Zhao, W.; Zhang, D.; Yan, C.; Li, W.; Liu, X.; Lu, Y.; Kirman, J.; Sargent, E. H.; Xiong, Q.; Wei, Z. Perovskite Light-Emitting Diodes with External Quantum Efficiency Exceeding 20 Per Cent. *Nature* **2018**, *562*, 245–248.
- (6) Zhang, Q.; Tavakoli, M. M.; Gu, L.; Zhang, D.; Tang, L.; Gao, Y.; Guo, J.; Lin, Y.; Leung, S.-F.; Poddar, S.; Fu, Y.; Fan, Z. Efficient Metal Halide Perovskite Light-Emitting Diodes with Significantly Improved Light Extraction on Nanophotonic Substrates. *Nat. Commun.* **2019**, *10*, 727.
- (7) Zhang, D.; Gu, L.; Zhang, Q.; Lin, Y.; Lien, D.-H.; Kam, M.; Poddar, S.; Garnett, E. C.; Javey, A.; Fan, Z. Increasing Photoluminescence Quantum Yield by Nanophotonic Design of Quantum-Confined Halide Perovskite Nanowire Arrays. *Nano Lett.* **2019**, *19*, 2850–2857.
- (8) Jeon, S.; Zhao, L.; Jung, Y. J.; Kim, J. W.; Kim, S. Y.; Kang, H.; Jeong, J. H.; Rand, B. P.; Lee, J. H. Perovskite Light-Emitting Diodes with Improved Outcoupling Using a High-Index Contrast Nanoarray. *Small* **2019**, *15*, 1900135.
- (9) Zhao, L.; Lee, K. M.; Roh, K.; Khan, S. U. Z.; Rand, B. P. Improved Outcoupling Efficiency and Stability of Perovskite Light-Emitting Diodes Using Thin Emitting Layers. *Adv. Mater.* **2019**, *31*, 1805836.
- (10) Shen, Y.; Cheng, L. P.; Li, Y. Q.; Li, W.; Chen, J. D.; Lee, S. T.; Tang, J. X. High-Efficiency Perovskite Light-Emitting Diodes with Synergetic Outcoupling Enhancement. *Adv. Mater.* **2019**, 1901517.
- (11) Song, J.; Kim, K.-H.; Kim, E.; Moon, C.-K.; Kim, Y.-H.; Kim, J.-J.; Yoo, S. Lensfree OLEDs with over 50% External Quantum Efficiency via External Scattering and Horizontally Oriented Emitters. *Nat. Commun.* **2018**, *9*, 3207.
- (12) Xu, W.; Hu, Q.; Bai, S.; Bao, C.; Miao, Y.; Yuan, Z.; Borzda, T.; Barker, A. J.; Tyukalova, E.; Hu, Z.; et al. Rational Molecular Passivation for High-Performance Perovskite Light-Emitting Diodes. *Nat. Photonics* **2019**, *13*, 418–424.

- (13) Zhao, B.; Bai, S.; Kim, V.; Lamboll, R.; Shivanna, R.; Auras, F.; Richter, J. M.; Yang, L.; Dai, L.; Alsari, M.; et al. High-Efficiency Perovskite–Polymer Bulk Heterostructure Light-Emitting Diodes. *Nat. Photonics* **2018**, *12*, 783–789.
- (14) Chiba, T.; Hayashi, Y.; Ebe, H.; Hoshi, K.; Sato, J.; Sato, S.; Pu, Y.-J.; Ohisa, S.; Kido, J. Anion-Exchange Red Perovskite Quantum Dots with Ammonium Iodine Salts for Highly Efficient Light-Emitting Devices. *Nat. Photonics* **2018**, *12*, 681–687.
- (15) Zou, W.; Li, R.; Zhang, S.; Liu, Y.; Wang, N.; Cao, Y.; Miao, Y.; Xu, M.; Guo, Q.; Di, D.; et al. Minimising Efficiency Roll-Off in High-Brightness Perovskite Light-Emitting Diodes. *Nat. Commun.* **2018**, *9*, 608.
- (16) Yan, R.; Gargas, D.; Yang, P. Nanowire Photonics. *Nat. Photonics* **2009**, *3*, 569–576.
- (17) Motohisa, J.; Kohashi, Y.; Maeda, S. Far-Field Emission Patterns of Nanowire Light-Emitting Diodes. *Nano Lett.* **2014**, *14*, 3653–3660.
- (18) Huttunen, M. J.; Dolgaleva, K.; Törmä, P.; Boyd, R. W. Ultra-Strong Polarization Dependence of Surface Lattice Resonances with Out-of-Plane Plasmon Oscillations. *Opt. Express* **2016**, *24*, 28279–28289.
- (19) Cao, L.; Fan, P.; Brongersma, M. L. Optical Coupling of Deep-Subwavelength Semiconductor Nanowires. *Nano Lett.* **2011**, *11*, 1463–1468.
- (20) Brongersma, M. L.; Cui, Y.; Fan, S. Light Management for Photovoltaics Using High-Index Nanostructures. *Nat. Mater.* **2014**, *13*, 451–460.
- (21) Landreman, P. E.; Chalabi, H.; Park, J.; Brongersma, M. L. Fabry-Perot Description for Mie Resonances of Rectangular Dielectric Nanowire Optical Resonators. *Opt. Express* **2016**, *24*, 29760–29772.
- (22) Kim, S.; Kim, K.-H.; Hill, D. J.; Park, H.-G.; Cahoon, J. F.; et al. Mie-Coupled Bound Guided States in Nanowire Geometric Superlattices. *Nat. Commun.* **2018**, *9*, 2781.
- (23) Abujetas, D. R.; Mandujano, M. A.; Méndez, E. R.; Sánchez-Gil, J. A. High-Contrast Fano Resonances in Single Semiconductor Nanorods. *ACS Photonics* **2017**, *4*, 1814–1821.
- (24) Alias, M. S.; Dursun, I.; Saidaminov, M. I.; Diallo, E. M.; Mishra, P.; Ng, T. K.; Bakr, O. M.; Ooi, B. S. Optical Constants of $\text{CH}_3\text{NH}_3\text{PbBr}_3$ Perovskite Thin Films Measured by Spectroscopic Ellipsometry. *Opt. Express* **2016**, *24*, 16586–16594.
- (25) Waleed, A.; Tavakoli, M. M.; Gu, L.; Wang, Z.; Zhang, D.; Manikandan, A.; Zhang, Q.; Zhang, R.; Chueh, Y.-L.; Fan, Z. Lead-Free Perovskite Nanowire Array Photodetectors with Drastically Improved Stability in Nanoengineering Templates. *Nano Lett.* **2017**, *17*, 523–530.
- (26) Waleed, A.; Fan, Z. Fabrication of Stable Organometallic Halide Perovskite NWs Based Optoelectronic Devices. *Sci. Bull.* **2017**, *62*, 645–647.
- (27) Yang, X.; Zhang, X.; Deng, J.; Chu, Z.; Jiang, Q.; Meng, J.; Wang, P.; Zhang, L.; Yin, Z.; You, J. Efficient Green Light-Emitting Diodes Based on Quasi-Two-Dimensional Composition and Phase Engineered Perovskite with Surface Passivation. *Nat. Commun.* **2018**, *9*, 570.
- (28) Kim, H.; Zhao, L.; Price, J. S.; Grede, A. J.; Roh, K.; Brigeman, A. N.; Lopez, M.; Rand, B. P.; Giebink, N. C. Hybrid Perovskite Light Emitting Diodes under Intense Electrical Excitation. *Nat. Commun.* **2018**, *9*, 4893.
- (29) Wei, Z.; Perumal, A.; Su, R.; Sushant, S.; Xing, J.; Zhang, Q.; Tan, S. T.; Demir, H. V.; Xiong, Q. Solution-Processed Highly Bright and Durable Cesium Lead Halide Perovskite Light-Emitting Diodes. *Nanoscale* **2016**, *8*, 18021–18026.
- (30) Handa, T.; Tahara, H.; Aharen, T.; Kanemitsu, Y. Large Negative Thermo-Optic Coefficients of a Lead Halide Perovskite. *Sci. Adv.* **2019**, *5*, No. eaax0786.
- (31) Gu, L.; Tavakoli, M. M.; Zhang, D.; Zhang, Q.; Waleed, A.; Xiao, Y.; Tsui, K. H.; Lin, Y.; Liao, L.; Wang, J.; et al. 3D Arrays of 1024-Pixel Image Sensors Based on Lead Halide Perovskite Nanowires. *Adv. Mater.* **2016**, *28*, 9713–9721.
- (32) Leung, S.-F.; Gu, L.; Zhang, Q.; Tsui, K.-H.; Shieh, J.-M.; Shen, C.-H.; Hsiao, T.-H.; Hsu, C.-H.; Lu, L.; Li, D.; et al. Roll-to-Roll Fabrication of Large Scale and Regular Arrays of Three-Dimensional Nanospikes for High Efficiency and Flexible Photovoltaics. *Sci. Rep.* **2015**, *4*, 4243.
- (33) Leung, S.-F.; Tsui, K.-H.; Lin, Q.; Huang, H.; Lu, L.; Shieh, J.-M.; Shen, C.-H.; Hsu, C.-H.; Zhang, Q.; Li, D.; et al. Large Scale, Flexible and Three-Dimensional Quasi-Ordered Aluminum Nanospikes for Thin Film Photovoltaics with Omnidirectional Light Trapping and Optimized Electrical Design. *Energy Environ. Sci.* **2014**, *7*, 3611–3616.
- (34) Oener, S. Z.; Khoram, P.; Brittan, S.; Mann, S. A.; Zhang, Q.; Fan, Z.; Boettcher, S. W.; Garnett, E. C. Perovskite Nanowire Extrusion. *Nano Lett.* **2017**, *17*, 6557–6563.
- (35) Khoram, P.; Oener, S. Z.; Zhang, Q.; Fan, Z.; Garnett, E. C. Surface Recombination Velocity of Methylammonium Lead Bromide Nanowires in Anodic Aluminium Oxide Templates. *Mol. Syst. Des. Eng.* **2018**, *3*, 723–728.
- (36) Shen, Y.; Cheng, L. P.; Li, Y. Q.; Li, W.; Chen, J. D.; Lee, S. T.; Tang, J. X. High-Efficiency Perovskite Light-Emitting Diodes with Synergetic Outcoupling Enhancement. *Adv. Mater.* **2019**, *31*, 1901517.